

# Neutron-rich nuclei and neutron skins from chiral low-resolution interactions

P. Arthuis,<sup>1,2,\*</sup> K. Hebeler,<sup>1,2,3,†</sup> and A. Schwenk<sup>1,2,3,‡</sup>

<sup>1</sup>*Technische Universität Darmstadt, Department of Physics, 64289 Darmstadt, Germany*

<sup>2</sup>*ExtreMe Matter Institute EMMI, GSI Helmholtzzentrum für Schwerionenforschung GmbH, 64291 Darmstadt, Germany*

<sup>3</sup>*Max-Planck-Institut für Kernphysik, Saupfercheckweg 1, 69117 Heidelberg, Germany*

Neutron-rich nuclei provide important insights to nuclear forces and to the nuclear equation of state. Advances in *ab initio* methods combined with new opportunities with rare isotope beams enable unique explorations of their properties based on nuclear forces applicable over the entire nuclear chart. In this Letter, we develop novel chiral low-resolution interactions that accurately describe bulk properties from  $^{16}\text{O}$  to  $^{208}\text{Pb}$ . With these, we investigate density distributions and neutron skins of neutron-rich nuclei. Our results show that neutron skins are narrowly predicted over all nuclei with interesting sensitivities for the most extreme, experimentally unexplored cases.

*Introduction.*– Neutron-rich nuclei constitute natural laboratories at the intersection of nuclear physics and astrophysics. Away from the valley of stability, shell structure evolves and neutron-rich nuclei become sensitive to important parts of nuclear forces [1–3]. The larger isospin asymmetry also offers natural connections to the nuclear equation of state and infinite matter in neutron stars. At the most neutron-rich extremes, nuclei are key for the *r*-process and nucleosynthesis [4]. As a result, neutron-rich nuclei constitute the main science driver for rare isotope beam facilities such as FAIR, FRIB, and RIBF. Simultaneously, advances in *ab initio* methods [5, 6] extended their reach up to  $^{208}\text{Pb}$  [7–9]. This offers tremendous perspectives of mutual feedback between theoretical and experimental efforts in the years to come.

Neutron skins have been a key focus for neutron-rich nuclei. In particular, the recent extraction of a large  $^{208}\text{Pb}$  neutron skin from parity-violating electron scattering [10], albeit with large uncertainties, has sparked intense discussions within the nuclear physics and astrophysics communities (see, e.g., Refs. [8, 11–13]). Through their correlations with the nuclear equation of state, neutron skins constitute an important connection between nuclei and dense matter in neutron stars. Because the neutron skin increases with isospin asymmetry, the upcoming experimental access to many unexplored neutron-rich nuclei paves the way for discoveries critical to our understanding of both finite and infinite nuclear systems.

The description of atomic nuclei from first principles is based on the development of nuclear interactions, many-body methods, and advances in scientific computing. The use of interactions based on chiral effective field theory (EFT) [14–17] and polynomially scaling many-body methods [18–21] has allowed for a rapid extension of the reach of *ab initio* methods both in terms of mass number  $A$  and of observables of interest. For applications across the nuclear chart, low-resolution interactions, either fit with a low-momentum cutoff  $\Lambda$  or obtained from a similarity renormalization group (SRG) evolution [22, 23] have proven especially successful [24–28]. In particular, they offer good convergence properties with respect to both model space size and expansion order of the many-body

method. This makes them key for exploring nuclei at the frontier of the current *ab initio* reach. In particular, the 1.8/2.0 (EM) two- and three-nucleon (NN+3N) interaction [24] has been widely used for studies of ground and excited states up to heavy nuclei [7, 9, 29, 30], but suffers from underprediction of radii [31]. As such, it appears critical to develop low-resolution interactions with good convergence properties and yielding a good reproduction of bulk properties of nuclei.

*Novel low-resolution interactions.*– To this end, we explore low-resolution NN+3N interactions following the strategy of Ref. [24]. This consists in evolving the NN interactions to the resolution scale  $\lambda = 1.8\text{ fm}^{-1}$  using the SRG and fitting the 3N low-energy couplings (LECs) at next-to-next-to-leading order ( $\text{N}^2\text{LO}$ ) with a cutoff  $\Lambda_{3\text{N}} = 2.0\text{ fm}^{-1}$  to few- and many-body observables. In this work we investigate the  $\text{N}^3\text{LO}$  EM 500 potential [32] used in Ref. [24] as well as the EMN [33] and NNLOsim [34] families. The NN SRG evolution has the advantage that the accurate reproduction of NN phase shifts is preserved [35]. The long-range LECs  $c_i$  of the 3N interactions are kept consistent with the corresponding NN potentials. In addition, we constrain the shorter-range 3N LECs  $c_D$  and  $c_E$  to reproduce the  $^3\text{H}$  ground-state energy [36]. In the present work, we use the ground-state energy and charge radius of  $^{16}\text{O}$  as a second constraint for  $c_D$ , in contrast to the  $^4\text{He}$  radius used in Ref. [24].

All many-body results presented in this work are calculated using the *ab initio* in-medium similarity renormalization group (IMSRG) [20] in the IMSRG(2) approximation, i.e., at the normal-ordered two-body level based on a Hartree-Fock reference state. The nuclear Hamiltonian is represented in a spherical harmonic-oscillator basis of size  $e_{\text{max}} = \max(2n + l) = 14$ , where  $n$  is the radial quantum number and  $l$  the orbital angular momentum. Matrix elements of the 3N forces are represented in a basis defined by  $e_1 + e_2 + e_3 \leq E_{\text{max}}^{(3)}$  with  $E_{\text{max}}^{(3)} = 24$  [7]. The harmonic-oscillator frequency  $\hbar\omega$  is selected to yield the best converged result depending on the system and observable, and ranges from 10 to 16 MeV.

Figure 1 shows the ground-state energy and charge

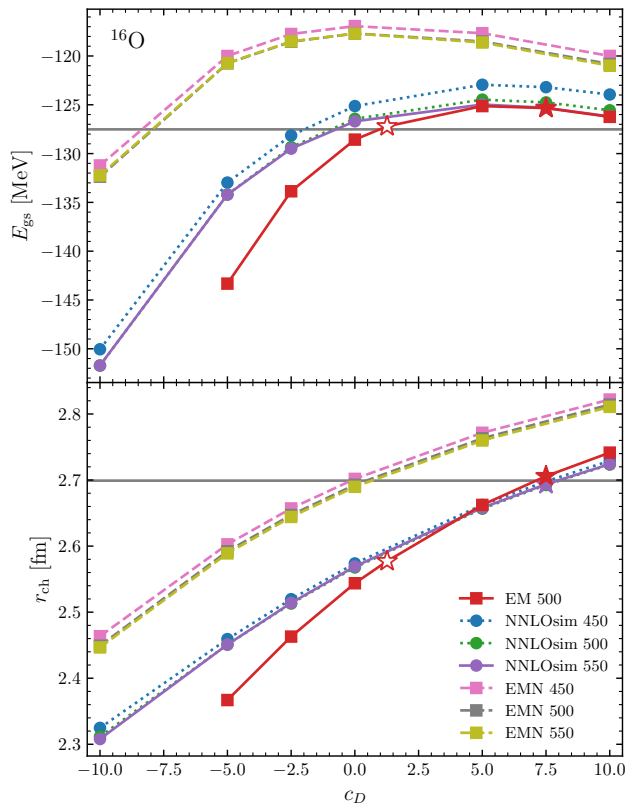


Figure 1. Ground-state energy (top panel) and charge radius (bottom panel) of  $^{16}\text{O}$  as a function of  $c_D$  for the low-resolution NN+3N interactions at NN SRG resolution scale  $\lambda = 1.8 \text{ fm}^{-1}$ . Horizontal grey lines correspond to the experimental values [37, 38]. The solid stars indicate the results corresponding to the two novel interactions 1.8/2.0 (EM7.5) and 1.8/2.0 (sim7.5), while the open star corresponds to the 1.8/2.0 (EM) interaction [24].

radius of  $^{16}\text{O}$  as a function of  $c_D$  for the different low-resolution NN+3N interactions. In all cases we find a rather strong sensitivity of the ground-state energy (upper panel) for negative  $c_D$  values, whereas for positive  $c_D$  the energy is rather insensitive to changes of the LEC. While the NNLOsim family and EM 500 potential show a very good agreement with experiment at positive  $c_D$ , the EMN family exhibits larger deviations. For the charge radius (lower panel) we find an almost linear dependence and increasing radii for larger  $c_D$  values. In particular, around  $c_D = 7.5$  the SRG-evolved NNLOsim and EM 500 interactions simultaneously reproduce both observables very well. On the other hand, the EMN interactions reproduce the experimental charge radius of  $^{16}\text{O}$  for a value of  $c_D \sim 0$ . However, here it is not possible to reproduce both observables simultaneously. Therefore, we selected two novel low-resolution interactions based on the EM 500 and NNLOsim 550 with a 3N LEC  $c_D = 7.5$  [39], that we named 1.8/2.0 (EM7.5) and 1.8/2.0 (sim7.5), respectively. As can be seen in Fig. 1, both these two

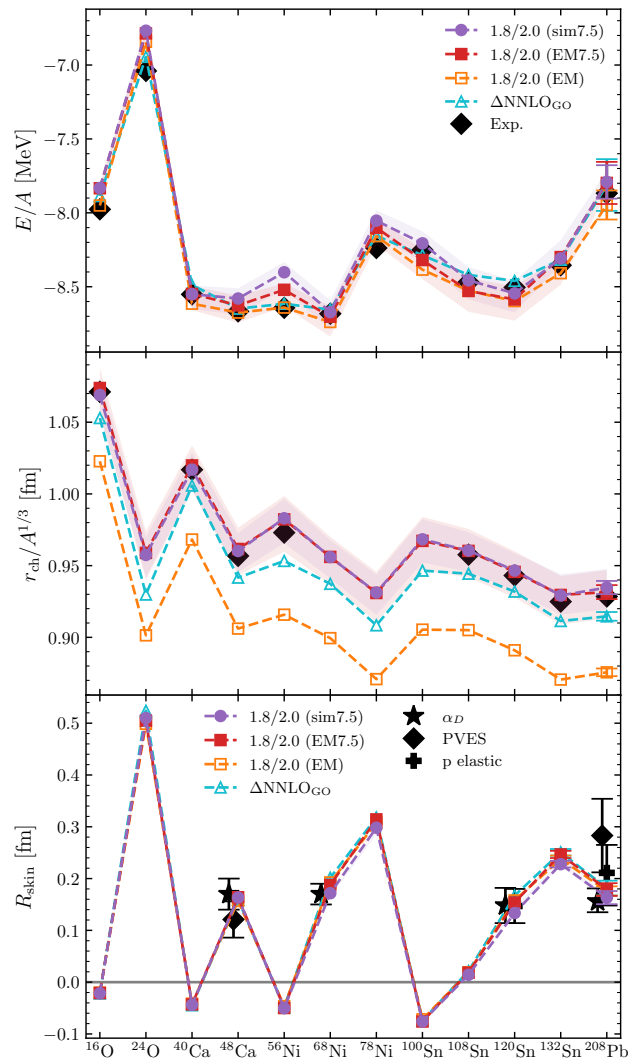


Figure 2. Ground-state energies per nucleon, charge radii, and neutron skins for selected doubly closed-shell nuclei from  $^{16}\text{O}$  to  $^{208}\text{Pb}$  compared with experiment for the two novel interactions 1.8/2.0 (EM7.5) and 1.8/2.0 (sim7.5) as well as the 1.8/2.0 (EM) and  $\Delta\text{NNLO}_{\text{GO}}$  interactions. Charge radii are scaled by  $A^{1/3}$  for legibility. Experimental data for neutron skins was obtained through dipole polarizability ( $\alpha_D$ ), parity-violating electron scattering (PVES), and elastic proton scattering (p elastic). See text for experimental references and for a discussion of the theoretical uncertainties given.

interactions, indicated by a solid star, predict essentially the same binding energies as the 1.8/2.0 (EM) interaction (marked by an open star), but resolve the problem of too small charge radii. This observation also holds for  $^{40}\text{Ca}$ , see the Supplemental Material.

*Ground-state energies, radii, and neutron skins.*— Figure 2 shows the ground-state energy and charge radius for selected doubly closed-shell nuclei ranging from  $^{16}\text{O}$  to  $^{208}\text{Pb}$  based on our novel low-resolution interactions as well as the established 1.8/2.0 (EM) [24] and

$\Delta\text{NNLO}_{\text{GO}}$  ( $\Lambda_{3\text{N}} = 394\text{ MeV}$ ) interactions [28]. For both 1.8/2.0 (EM7.5) and 1.8/2.0 (sim7.5), the bands are obtained by varying  $c_D$  from 5 to 10 and represent an uncertainty estimate associated to our choice of  $c_D$  value. The top panel displays ground-state energies per nucleon compared to experimental values from Ref. [37]. All interactions show good agreement over the entire range, with deviations from experiment below 2% [40]. In the case of  $^{208}\text{Pb}$ , our results were extrapolated assuming a geometric convergence with respect to  $e_{\text{max}}$  [41], and error bars correspond to change from  $e_{\text{max}} = 12$  to 14. The agreement with experiment is remarkably good, and thus establishes the new low-resolution interactions as very promising for *ab initio* studies across the nuclear chart. The central panel displays the charge radius scaled by  $A^{1/3}$ . Here the new interactions display a strikingly good agreement with experiment [38, 42], and in particular a significant improvement with respect to the 1.8/2.0 (EM) and  $\Delta\text{NNLO}_{\text{GO}}$  interactions. Finally, the bottom panel shows the neutron skin, defined as the difference between point-neutron and point-proton radii, compared to experimental extractions from the dipole polarizability [43–46], parity-violating electron scattering [10, 47], and elastic proton scattering [48, 49]. We find that the neutron skins are predicted remarkably similar for all interactions explored, even if the charge radii are underestimated from 1.8/2.0 (EM) and  $\Delta\text{NNLO}_{\text{GO}}$ . Our results also agree well with experiment, with the exception of the PREX result [10] for  $^{208}\text{Pb}$ , where the agreement is only within the  $2\sigma$  range. These results demonstrate the capability of our new low-resolution interactions for neutron skins, and thus can also be used in experimental analyses to provide constraints on the symmetry energy slope  $L$  [50].

*Density distributions.*— Density distributions offer insights into nuclear structure by combining a bulk description of the nucleus with information on the internal shell. With ample information for stable nuclei, electron scattering experiments on rare isotopes are also becoming possible [52]. Figure 3 displays the charge and point-neutron density distributions for  $^{120}\text{Sn}$ , a candidate system for the extraction of the symmetry energy slope  $L$  [50]. The darker theoretical uncertainty bands in Fig. 3 are obtained by varying the harmonic-oscillator frequency around the optimal value, while the lighter bands show the sensitivity of the results to changing  $e_{\text{max}}$  from 12 to 14. For comparison, we also show results based on the NNLOsat interaction [25], which proved to reproduce well the charge density distributions in the Sn region [53]. For these calculations we were able to make use of the novel matrix element storage scheme [7] to yield vastly reduced uncertainties compared to Ref. [53]. Results for the charge distribution show a good reproduction of two-point Fermi and three-point Gaussian parametrizations extracted from experiment [51], where differences could only be resolved through a more detailed experimental description. Interestingly, the behavior obtained for the

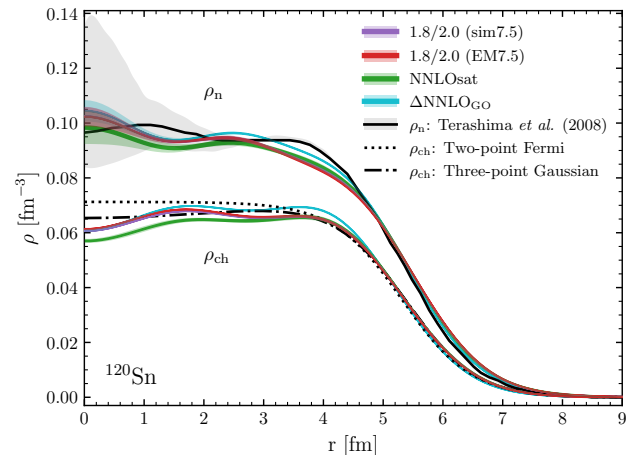


Figure 3. Charge and point-neutron density distributions for  $^{120}\text{Sn}$  for the two novel interactions 1.8/2.0 (EM7.5) and 1.8/2.0 (sim7.5) as well as the NNLOsat and  $\Delta\text{NNLO}_{\text{GO}}$  interactions, compared to experimental constraints [48, 51]. The darker and lighter theoretical uncertainty bands estimate the convergence by varying  $\hbar\omega$  and  $e_{\text{max}}$ , respectively.

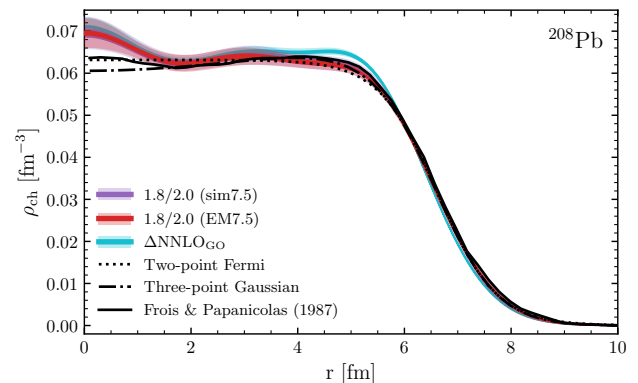


Figure 4. Charge density distribution for  $^{208}\text{Pb}$  for the two novel interactions 1.8/2.0 (EM7.5) and 1.8/2.0 (sim7.5) as well as the  $\Delta\text{NNLO}_{\text{GO}}$  interaction, compared to data compiled in Refs. [54, 55]. The theoretical uncertainties are as in Fig. 3.

novel 1.8/2.0 (EM7.5) and 1.8/2.0 (sim7.5) interactions are very similar. Results for the point-neutron density distribution exhibit larger uncertainties, especially in the core of the nucleus. Here the differences with the experimental extraction from Terashima *et al.* [48] are larger, with our *ab initio* results yielding a softer shoulder toward the neutron skin.

Figure 4 displays the charge density distribution for  $^{208}\text{Pb}$  compared to two-point Fermi and three-point Gaussian parametrizations [54] as well as the compiled data from Frois and Papanicolas [55]. The model-space convergence uncertainties remain moderate and overall the reproduction of experiment is very good. Our novel

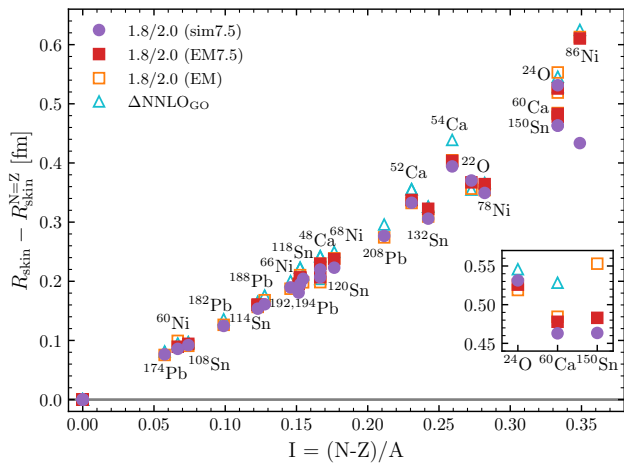


Figure 5. Neutron skin with respect to the corresponding  $N = Z$  isotope for selected doubly closed-shell nuclei as a function of the isospin asymmetry for the two novel interactions 1.8/2.0 (EM7.5) and 1.8/2.0 (sim7.5) as well as the 1.8/2.0 (EM) and  $\Delta\text{NNLO}_{\text{GO}}$  interactions.

1.8/2.0 (EM7.5) and 1.8/2.0 (sim7.5) interactions display very similar results, while  $\Delta\text{NNLO}_{\text{GO}}$  yields a slightly too compressed density with a stronger shoulder at larger distances. Note that convergence with model space cannot be obtained for the NNLOsat interaction for such heavy nuclei. Overall these results demonstrate the ability of chiral low-resolution interactions to reproduce density distributions over the whole nuclear chart and serve as valuable guidance for experimental campaigns.

*Isospin dependence of neutron skins.*— Neutron skins provide a direct connection between nuclei and the equation of state of neutron-rich matter through the symmetry energy slope  $L$  [8, 10–13, 43–47, 50, 56, 57]. Macroscopic models have linked the neutron skin thickness to the isospin asymmetry  $I = (N - Z)/A$  [58, 59], with the correlation being approximately linear. Such a correlation was recently confirmed with *ab initio* calculations for medium-mass nuclei [60]. We effectively subtract the Coulomb contribution by plotting  $R_{\text{skin}}$  relative to the (negative)  $R_{\text{skin}}^{N=Z}$  of the  $N = Z$  isotope in the chain. This is shown in Fig. 5 for selected closed-shell isotopes of O, Ca, Ni, Sn and Pb. We find that up to  $I \approx 0.2$  the growth in neutron skin thickness is linear with respect to  $I$  and all interactions yield very similar results, as already apparent for the nuclei studied in Fig. 2. However, for  $I \gtrsim 0.25$  nuclei show more scatter and thus a stronger sensitivity on the employed interaction [61]. The inset shows the results for the different nuclei at  $I = 1/3$  in more detail. These results indicate that very neutron-rich isotopes like  $^{60}\text{Ca}$ ,  $^{86}\text{Ni}$  or  $^{150}\text{Sn}$  are very interesting candidates to discriminate between nuclear interactions and better understand the link between neutron skins and the isospin asymmetry.

*Conclusions and outlook.*— In this Letter, we developed novel chiral low-resolution interactions based on SRG-evolved high-precision NN potentials combined with 3N forces at  $\text{N}^2\text{LO}$  fitted to the ground-state energies of  $^3\text{H}$  and  $^{16}\text{O}$  as well as the charge radius of  $^{16}\text{O}$ . The new interactions accurately reproduce experimental ground-state energies, charge radii, and neutron skins for closed-shell nuclei from  $^{16}\text{O}$  up to  $^{208}\text{Pb}$ , and hence resolve shortcomings of the established low-resolution interaction 1.8/2.0 (EM). The new interactions also predict density distributions for  $^{120}\text{Sn}$  and  $^{208}\text{Pb}$  in remarkable agreement with experiment. Finally, we investigated neutron skins for neutron-rich nuclei, a key quantity that links nuclei to infinite nuclear matter and astrophysics. We found that neutron skins are narrowly predicted over all nuclei with interesting sensitivities for the most extreme, experimentally unexplored cases. This motivates further investigations of neutron-rich nuclei with rare isotope beam facilities in order to obtain constraints for nuclear forces and to better understand the connection to the equation of state. Our novel low-resolution interactions present a powerful tool for comprehensive *ab initio* studies of the nuclear chart including open-shell nuclei as well as other observables like excited states or response functions to external probes.

We thank T. Aumann, M. Heinz, T. Miyagi, and A. Tichai for helpful discussions. Three-body matrix elements of the interactions were generated using the NuHamil code [62], and calculations using the IMSRG code from S. R. Stroberg [63]. This work was supported in part by the European Research Council (ERC) under the European Union’s Horizon 2020 research and innovation programme (Grant Agreement No. 101020842), the Deutsche Forschungsgemeinschaft (DFG, German Research Foundation) – Project-ID 279384907 – SFB 1245, and the Helmholtz Forschungsakademie Hessen für FAIR (HFHF). The authors gratefully acknowledge the Gauss Centre for Supercomputing e.V. ([www.gauss-centre.eu](http://www.gauss-centre.eu)) for funding this project by providing computing time through the John von Neumann Institute for Computing (NIC) on the GCS Supercomputer JUWELS at Jülich Supercomputing Centre (JSC).

\* [parthuis@theorie.ikp.physik.tu-darmstadt.de](mailto:parthuis@theorie.ikp.physik.tu-darmstadt.de)

† [kai.hebeler@physik.tu-darmstadt.de](mailto:kai.hebeler@physik.tu-darmstadt.de)

‡ [schwenk@physik.tu-darmstadt.de](mailto:schwenk@physik.tu-darmstadt.de)

- [1] K. Hebeler, J. D. Holt, J. Menéndez, and A. Schwenk, Nuclear Forces and Their Impact on Neutron-Rich Nuclei and Neutron-Rich Matter, *Annu. Rev. Nucl. Part. Sci.* **65**, 457 (2015).
- [2] T. Otsuka, A. Gade, O. Sorlin, T. Suzuki, and Y. Utsuno, Evolution of shell structure in exotic nuclei, *Rev. Mod. Phys.* **92**, 015002 (2020).

- [3] F. Nowacki, A. Obertelli, and A. Poves, The neutron-rich edge of the nuclear landscape: Experiment and theory., *Prog. Part. Nucl. Phys.* **120**, 103866 (2021).
- [4] H. Schatz, A. D. Becerril Reyes, A. Best, E. F. Brown, K. Chatziioannou, K. A. Chipps, C. M. Deibel, R. Ezzeddine, D. K. Galloway, C. J. Hansen, *et al.*, Horizons: nuclear astrophysics in the 2020s and beyond, *J. Phys. G* **49**, 110502 (2022).
- [5] H. Hergert, A Guided Tour of *ab initio* Nuclear Many-Body Theory, *Front. Phys.* **8**, 379 (2020).
- [6] K. Hebeler, Three-nucleon forces: Implementation and applications to atomic nuclei and dense matter, *Phys. Rep.* **890**, 1 (2021).
- [7] T. Miyagi, S. R. Stroberg, P. Navrátil, K. Hebeler, and J. D. Holt, Converged *ab initio* calculations of heavy nuclei, *Phys. Rev. C* **105**, 014302 (2022).
- [8] B. Hu *et al.*, *Ab initio* predictions link the neutron skin of  $^{208}\text{Pb}$  to nuclear forces, *Nat. Phys.* **18**, 1196 (2022).
- [9] K. Hebeler, V. Durant, J. Hoppe, M. Heinz, A. Schwenk, J. Simonis, and A. Tichai, Normal ordering of three-nucleon interactions for *ab initio* calculations of heavy nuclei, *Phys. Rev. C* **107**, 024310 (2023).
- [10] D. Adhikari *et al.* (PREX Collaboration), Accurate determination of the neutron skin thickness of  $^{208}\text{Pb}$  through parity-violation in electron scattering, *Phys. Rev. Lett.* **126**, 172502 (2021).
- [11] R. Essick, I. Tews, P. Landry, and A. Schwenk, Astrophysical Constraints on the Symmetry Energy and the Neutron Skin of  $^{208}\text{Pb}$  with Minimal Modeling Assumptions, *Phys. Rev. Lett.* **127**, 192701 (2021).
- [12] P.-G. Reinhard, X. Roca-Maza, and W. Nazarewicz, Combined Theoretical Analysis of the Parity-Violating Asymmetry for  $^{48}\text{Ca}$  and  $^{208}\text{Pb}$ , *Phys. Rev. Lett.* **129**, 232501 (2022).
- [13] J. M. Mamei, C. J. Horowitz, J. Piekarewicz, B. Reed, and C. Sfienti, Neutron Skins: Weak Elastic Scattering and Neutron Stars, [arXiv:2311.06146 \[nucl-th\]](https://arxiv.org/abs/2311.06146).
- [14] E. Epelbaum, H.-W. Hammer, and U.-G. Meißner, Modern theory of nuclear forces, *Rev. Mod. Phys.* **81**, 1773 (2009).
- [15] D. Rodriguez Entem, R. Machleidt, and Y. Nosyk, Nucleon-Nucleon Scattering Up to  $\text{N}^5\text{LO}$  in Chiral Effective Field Theory, *Front. Phys.* **8**, 57 (2020).
- [16] E. Epelbaum, H. Krebs, and P. Reinert, High-precision nuclear forces from chiral EFT: State-of-the-art, challenges and outlook, *Front. Phys.* **8**, 98 (2020).
- [17] H.-W. Hammer, S. König, and U. van Kolck, Nuclear effective field theory: Status and perspectives, *Rev. Mod. Phys.* **92**, 025004 (2020).
- [18] G. Hagen, T. Papenbrock, M. Hjorth-Jensen, and D. J. Dean, Coupled-cluster computations of atomic nuclei, *Rep. Prog. Phys.* **77**, 096302 (2014).
- [19] V. Somà, A. Cipollone, C. Barbieri, P. Navrátil, and T. Duguet, Chiral two- and three-nucleon forces along medium-mass isotope chains, *Phys. Rev. C* **89**, 061301(R) (2014).
- [20] H. Hergert, S. K. Bogner, T. D. Morris, A. Schwenk, and K. Tsukiyama, The In-Medium Similarity Renormalization Group: A novel *ab initio* method for nuclei, *Phys. Rep.* **621**, 165 (2016).
- [21] A. Tichai, R. Roth, and T. Duguet, Many-Body Perturbation Theories for Finite Nuclei, *Front. Phys.* **8**, 164 (2020).
- [22] S. K. Bogner, R. J. Furnstahl, and R. J. Perry, Similarity Renormalization Group for Nucleon-Nucleon Interactions, *Phys. Rev. C* **75**, 061001(R) (2007).
- [23] R. J. Furnstahl and K. Hebeler, New applications of renormalization group methods in nuclear physics, *Rep. Prog. Phys.* **76**, 126301 (2013).
- [24] K. Hebeler, S. K. Bogner, R. J. Furnstahl, A. Nogga, and A. Schwenk, Improved nuclear matter calculations from chiral low-momentum interactions, *Phys. Rev. C* **83**, 031301(R) (2011).
- [25] A. Ekström, G. R. Jansen, K. A. Wendt, G. Hagen, T. Papenbrock, B. D. Carlsson, C. Forssén, M. Hjorth-Jensen, P. Navrátil, and W. Nazarewicz, Accurate nuclear radii and binding energies from a chiral interaction, *Phys. Rev. C* **91**, 051301(R) (2015).
- [26] T. Hübner, K. Vobig, K. Hebeler, R. Machleidt, and R. Roth, Family of chiral two- plus three-nucleon interactions for accurate nuclear structure studies, *Phys. Lett. B* **808**, 135651 (2020).
- [27] V. Somà, P. Navrátil, F. Raimondi, C. Barbieri, and T. Duguet, Novel chiral Hamiltonian and observables in light and medium-mass nuclei, *Phys. Rev. C* **101**, 014318 (2020).
- [28] W. G. Jiang, A. Ekström, C. Forssén, G. Hagen, G. R. Jansen, and T. Papenbrock, Accurate bulk properties of nuclei from  $A = 2$  to  $\infty$  from potentials with  $\Delta$  isobars, *Phys. Rev. C* **102**, 054301 (2020).
- [29] T. D. Morris, J. Simonis, S. R. Stroberg, C. Stumpf, G. Hagen, J. D. Holt, G. R. Jansen, T. Papenbrock, R. Roth, and A. Schwenk, Structure of the Lightest Tin Isotopes, *Phys. Rev. Lett.* **120**, 152503 (2018).
- [30] S. R. Stroberg, J. D. Holt, A. Schwenk, and J. Simonis, *Ab Initio* Limits of Atomic Nuclei, *Phys. Rev. Lett.* **126**, 022501 (2021).
- [31] J. Simonis, S. R. Stroberg, K. Hebeler, J. D. Holt, and A. Schwenk, Saturation with chiral interactions and consequences for finite nuclei, *Phys. Rev. C* **96**, 014303 (2017).
- [32] D. R. Entem and R. Machleidt, Accurate charge-dependent nucleon-nucleon potential at fourth order of chiral perturbation theory, *Phys. Rev. C* **68**, 041001(R) (2003).
- [33] D. R. Entem, R. Machleidt, and Y. Nosyk, High-quality two-nucleon potentials up to fifth order of the chiral expansion, *Phys. Rev. C* **96**, 024004 (2017).
- [34] B. D. Carlsson, A. Ekström, C. Forssén, D. F. Strömberg, G. R. Jansen, O. Lilja, M. Lindby, B. A. Mattsson, and K. A. Wendt, Uncertainty analysis and order-by-order optimization of chiral nuclear interactions, *Phys. Rev. X* **6**, 011019 (2016).
- [35] S. K. Bogner, R. J. Furnstahl, and A. Schwenk, From low-momentum interactions to nuclear structure, *Prog. Part. Nucl. Phys.* **65**, 94 (2010).
- [36] See Supplemental Material for a detailed discussion of the developed chiral low-resolution interactions,  $^3\text{H}$  fits, and properties in many-body systems.
- [37] M. Wang, W. J. Huang, F. G. Kondev, G. Audi, and S. Naimi, The AME 2020 atomic mass evaluation II. Tables, graphs and references, *Chin. Phys. C* **45**, 030003 (2021).
- [38] I. Angeli and K. P. Marinova, Table of experimental nuclear ground state charge radii: An update, *At. Data Nucl. Data Tables* **99**, 69 (2013).
- [39] While this value of  $c_D$  appears particularly large, it is consistent with previous fits of SRG-evolved low-cutoff

- interactions [26].
- [40] The only exception is  $^{56}\text{Ni}$  with the 1.8/2.0 (sim7.5) interaction, where the deviation is associated to an anomalously low third-order many-body perturbation theory correction.
- [41] We obtain the extrapolated ground-state energy as follows,  $E_{\text{gs}} = E_{\text{gs}}(e_{\text{max}} = 12) + \delta E_{\text{gs}}^{14} / [1 - (\delta E_{\text{gs}}^{14} - \delta E_{\text{gs}}^{12})]$  with  $\delta E_{\text{gs}}^n = E_{\text{gs}}(e_{\text{max}} = n) - E_{\text{gs}}(e_{\text{max}} = n - 2)$ .
- [42] F. Sommer, K. König, D. M. Rossi, N. Everett, D. Garand, R. P. de Groote, J. D. Holt, P. Imgram, A. Incorvati, C. Kalman, *et al.*, Charge Radii of  $^{55,56}\text{Ni}$  Reveal a Surprisingly Similar Behavior at  $N = 28$  in Ca and Ni Isotopes, *Phys. Rev. Lett.* **129**, 132501 (2022).
- [43] J. Birkhan, M. Miorelli, S. Bacca, S. Bassauer, C. A. Bertulani, G. Hagen, H. Matsubara, P. von Neumann-Cosel, T. Papenbrock, N. Pietralla, *et al.*, Electric dipole polarizability of  $^{48}\text{Ca}$  and implications for the neutron skin, *Phys. Rev. Lett.* **118**, 252501 (2017).
- [44] D. M. Rossi *et al.*, Measurement of the Dipole Polarizability of the Unstable Neutron-Rich Nucleus  $^{68}\text{Ni}$ , *Phys. Rev. Lett.* **111**, 242503 (2013).
- [45] T. Hashimoto *et al.*, Dipole polarizability of  $^{120}\text{Sn}$  and nuclear energy density functionals, *Phys. Rev. C* **92**, 031305(R) (2015).
- [46] A. Tamii, I. Poltoratska, P. von Neumann-Cosel, Y. Fujita, T. Adachi, *et al.*, Complete electric dipole response and the neutron skin in  $^{208}\text{Pb}$ , *Phys. Rev. Lett.* **107**, 062502 (2011).
- [47] D. Adhikari *et al.* (CREX Collaboration), Precision Determination of the Neutral Weak Form Factor of  $^{48}\text{Ca}$ , *Phys. Rev. Lett.* **129**, 042501 (2022).
- [48] S. Terashima, H. Sakaguchi, H. Takeda, T. Ishikawa, M. Itoh, T. Kawabata, T. Murakami, M. Uchida, Y. Yasuda, M. Yosoi, *et al.*, Proton elastic scattering from tin isotopes at 295 MeV and systematic change of neutron density distributions, *Phys. Rev. C* **77**, 024317 (2008).
- [49] J. Zenihiro *et al.*, Neutron density distributions of  $^{204,206,208}\text{Pb}$  deduced via proton elastic scattering at  $E_p = 295$  MeV, *Phys. Rev. C* **82**, 044611 (2010).
- [50] T. Aumann, C. A. Bertulani, F. Schindler, and S. Typel, Peeling Off Neutron Skins from Neutron-Rich Nuclei: Constraints on the Symmetry Energy from Neutron-Removal Cross Sections, *Phys. Rev. Lett.* **119**, 262501 (2017).
- [51] H. De Vries, C. W. De Jager, and C. De Vries, Nuclear charge and magnetization density distribution parameters from elastic electron scattering, *At. Data Nucl. Data Tables* **36**, 495 (1987).
- [52] K. Tsukada, A. Enokizono, T. Ohnishi, K. Adachi, T. Fujita, M. Hara, M. Hori, T. Hori, S. Ichikawa, K. Kurita, *et al.*, First Elastic Electron Scattering from  $^{132}\text{Xe}$  at the SCRIT Facility, *Phys. Rev. Lett.* **118**, 262501 (2017).
- [53] P. Arthuis, C. Barbieri, M. Vorabbi, and P. Finelli, *Ab initio* computation of charge densities for Sn and Xe isotopes, *Phys. Rev. Lett.* **125**, 182501 (2020).
- [54] C. W. De Jager, H. De Vries, and C. De Vries, Nuclear charge and magnetization density distribution parameters from elastic electron scattering, *At. Data Nucl. Data Tables* **14**, 479 (1974), [Erratum: *At. Data Nucl. Data Tables* **16**, 580 (1975)].
- [55] B. Frois and C. Papanicolas, Electron scattering and nuclear structure, *Annu. Rev. Nucl. Part. Sci.* **37**, 133 (1987).
- [56] X. Roca-Maza, X. Viñas, M. Centelles, B. K. Agrawal, G. Colò, N. Paar, J. Piekarewicz, and D. Vretenar, Neutron skin thickness from the measured electric dipole polarizability in  $^{68}\text{Ni}$ ,  $^{120}\text{Sn}$ , and  $^{208}\text{Pb}$ , *Phys. Rev. C* **92**, 064304 (2015).
- [57] F. Fattoyev, J. Piekarewicz, and C. Horowitz, Neutron Skins and Neutron Stars in the Multimessenger Era, *Phys. Rev. Lett.* **120**, 172702 (2018).
- [58] W. D. Myers and W. Swiatecki, Average nuclear properties, *Ann. Phys. (N. Y.)* **55**, 395 (1969).
- [59] J. M. Lattimer and Y. Lim, Constraining the Symmetry Parameters of the Nuclear Interaction, *Astrophys. J.* **771**, 51 (2013).
- [60] S. Novario, D. Lonardoni, S. Gandolfi, and G. Hagen, Trends of neutron skins and radii of mirror nuclei from first principles, *Phys. Rev. Lett.* **130**, 032501 (2023).
- [61] In the case of  $^{86}\text{Ni}$  and the 1.8/2.0 (sim7.5) interaction, the significantly smaller neutron skin is associated to an underbinding of the system with respect to other interactions, indicating a possible interaction deficiency for this specific system.
- [62] T. Miyagi, NuHamil: A numerical code to generate nuclear two- and three-body matrix elements from chiral effective field theory, *Eur. Phys. J. A* **59**, 150 (2023).
- [63] S. R. Stroberg, <https://github.com/ragnarstroberg/imsrg>.
- [64] M. Hoferichter, J. Ruiz de Elvira, B. Kubis, and U.-G. Meißner, Matching pion-nucleon Roy-Steiner equations to chiral perturbation theory, *Phys. Rev. Lett.* **115**, 192301 (2015).

## SUPPLEMENTAL MATERIAL

*Chiral low-resolution interactions.*— The results presented in this work are based on chiral low resolution NN+3N interactions derived following the strategy of Ref. [24]. Specifically, we start from a NN interaction that is evolved to lower resolution scales via the SRG, which leaves all two-body observables unchanged by construction. In a second step, the shorter-range 3N interactions are fitted at low resolution in combination with the SRG-evolved NN interaction to few-body observables, e.g., using the  ${}^3\text{H}$  binding energy and the  ${}^4\text{He}$  radius as was done in Ref. [24]. The LECs  $c_1$ ,  $c_3$ , and  $c_4$  of the long-range 3N interactions are chosen consistently with the values used in the corresponding NN interaction. This strategy assumes that the long-range parts of nuclear forces are unchanged by the SRG evolution, and that the chiral EFT interactions remain an adequate operator basis at low resolution. For the fits of the shorter-range LECs  $c_D$  and  $c_E$ , all 3N interactions are regulated with the 3N regulator  $f(p, q)$  (for details see below) and cutoff  $\Lambda_{3\text{N}} = 2.0 \text{ fm}^{-1}$ . This choice leads to excellent many-body convergence for medium-mass to heavy nuclei [7, 9, 29, 31]. Moreover, this strategy has led to the 1.8/2.0 (EM) NN+3N interaction [24], which exhibits remarkable agreement with experimental binding energies over a wide range of the nuclear chart (see, e.g., Refs. [30, 31]).

*Improved fits of low-resolution NN+3N interactions.*— Despite the successes of interactions fitted at low resolution, the Hamiltonians derived in Ref. [24] also exhibit shortcomings, in particular in form of too small charge radii of medium-mass and heavy nuclei compared to experiment. Hence, in this work we generalize this approach by extending the set of considered NN interactions and by including many-body observables in the fits. Specifically, we consider in addition to the  $\text{N}^3\text{LO}$  EM 500 NN potential [32] two more recent families of NN interactions: First, we explore the NNLOsim family of  $\text{N}^2\text{LO}$  potentials [34], where we focus on the interactions optimized to scattering energies up to  $T_{\text{Lab}}^{\text{max}} = 290 \text{ MeV}$ . Second, we use the EMN potentials of Ref. [33] at  $\text{N}^2\text{LO}$ , consistent with the order of the employed 3N interactions. For the EMN potentials the  $c_i$  LECs are fixed based on the Roy-Steiner analysis [64] of pion-nucleon scattering data, while for the NNLOsim potentials they are optimized to NN and 3N data. For both families of interactions we consider the three cutoff values  $\Lambda_{\text{NN}} = 450, 500$  and  $550 \text{ MeV}$ .

As in Ref. [24] we first constrain the two LECs  $c_D$  and  $c_E$  to the experimental binding energy of  ${}^3\text{H}$  by solving the bound-state Faddeev equations. Figure 6 shows the results for the low-resolution NN+3N interactions discussed above (with the NN potential SRG-evolved to the resolution scale  $\lambda = 1.8 \text{ fm}^{-1}$ ) as well as for the 1.8/2.0 (EM) interaction [24]. The relations between the two LECs are almost linear, indicating the perturbativeness

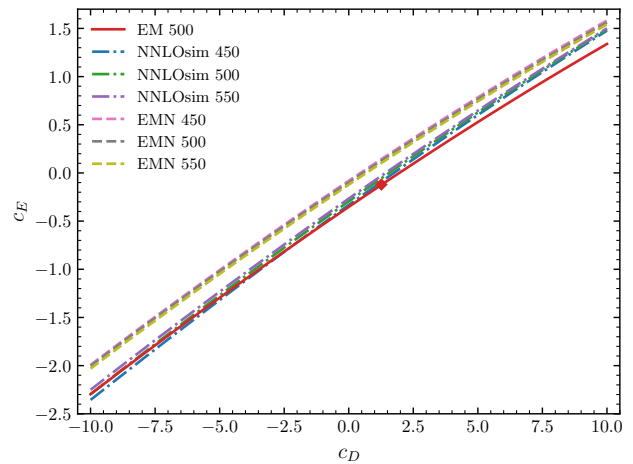


Figure 6. Three-nucleon LECs  $c_D$  and  $c_E$  that reproduce the  ${}^3\text{H}$  binding energy for the employed low-resolution NN+3N interactions at NN SRG resolution scale  $\lambda = 1.8 \text{ fm}^{-1}$ . The coupling values of the 1.8/2.0 (EM) interaction [24] are indicated by a red diamond for reference.

of these low-resolution interactions. Furthermore, within a given family of NN interactions the obtained trajectories are very close to each other. This is reminiscent of the NN universality at low resolution [35], so that the impact of the cutoff of the unevolved NN potential is small. In particular, we find almost identical results for the three EMN interactions, which all share the same  $c_i$  LECs. This demonstrates a high degree of universality of SRG-evolved NN interactions at this low resolution scale.

*Incorporation of many-body observables.*— Starting from the correlations shown in Fig. 6, we fix the values of the LECs based on the ground-state energy and charge radius of  ${}^{16}\text{O}$ . Figure 1 (in the main text) shows the predicted results as a function of  $c_D$  for the different 1.8/2.0 interactions. We find that for the NN potentials EM 500 and for the NNLOsim family, evolved to the resolution scale  $\lambda = 1.8 \text{ fm}^{-1}$ , it is possible to obtain a simultaneous fit of the  ${}^3\text{H}$  and  ${}^{16}\text{O}$  ground-state energies as well as the  ${}^{16}\text{O}$  charge radius using chiral  $\text{N}^2\text{LO}$  3N in-

Table I. 3N LECs for the 1.8/2.0 (EM) interaction [24] (left column) and the two novel low-resolution NN+3N interactions (middle and right columns). The interaction 1.8/2.0 (EM7.5) is based on the same  $\text{N}^3\text{LO}$  EM 500 NN potential [32] while 1.8/2.0 (sim7.5) is based on the NNLOsim NN potential [34] for  $T_{\text{Lab}}^{\text{max}} = 290 \text{ MeV}$  and  $\Lambda = 550 \text{ MeV}$ .

LEC	1.8/2.0 (EM)	1.8/2.0 (EM7.5)	1.8/2.0 (sim7.5)
$c_1$	-0.81	-0.81	0.27
$c_3$	-3.2	-3.2	-3.56
$c_4$	5.4	5.4	3.644
$c_D$	1.264	7.5	7.5
$c_E$	-0.12	0.942	1.081

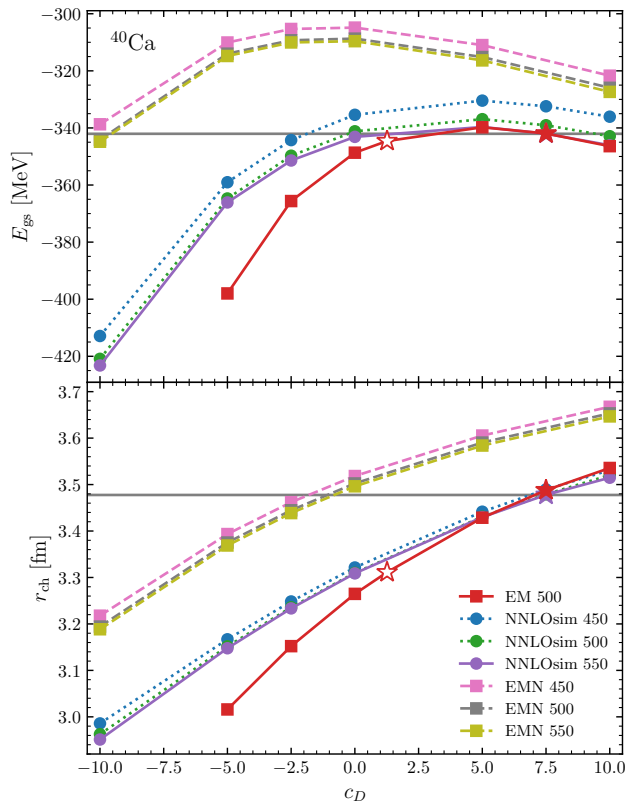


Figure 7. Ground-state energy (top panel) and charge radius (bottom panel) of  $^{40}\text{Ca}$  as a function of  $c_D$  for the low-resolution NN+3N interactions shown in Fig. 6. Horizontal grey lines correspond to the experimental values [37, 38]. The solid stars indicate the results corresponding to the two novel interactions 1.8/2.0 (EM7.5) and 1.8/2.0 (sim7.5), while the open star corresponds to the 1.8/2.0 (EM) interaction [24].

interactions with  $\Lambda_{3N} = 2.0 \text{ fm}^{-1}$ . The corresponding LECs of the 3N interactions are summarized in Tab. I. Figure 7 shows the corresponding results also hold for  $^{40}\text{Ca}$ . The fact that the low-resolution EMN interactions do not allow for a simultaneous fit of all three observables can be traced back to the  $c_i$  values. In particular, we observed that adjustments of  $c_4$  mainly affect the curvature of the parabola observed for both the  $^{16}\text{O}$  and  $^{40}\text{Ca}$  ground-state energy as a function of  $c_D$ , while  $c_1$  and  $c_3$  mostly lead to constant shifts of the energy and charge radius results. In addition, we also studied the sensitivity of the results to the shape of the 3N interaction regulator function  $f(p, q) = \exp[-((p^2 + \frac{3}{4}q^2)/\Lambda_{3N}^2)^{n_{\text{exp}}}]$  (with the Jacobi momenta  $p$  and  $q$  [6]), which is effectively controlled by  $n_{\text{exp}}$ . Different values have been employed for this parameter in recent works: While in Ref. [24] the value  $n_{\text{exp}} = 4$  was used, in Refs. [26, 34]  $n_{\text{exp}} = 3$  was used. In this work, we use  $n_{\text{exp}} = 4$ , except for the NNLOsim family, for which we kept the original choice  $n_{\text{exp}} = 3$ . However, investigating both values for NNLOsim, we found that these different choices have only a very small impact on the results and hence cannot explain the difference between the interactions.